

ACCEPTED VERSION

Xuegang Li, Stephen C. Warren-Smith, Heike Ebendorff-Heidepriem, Ya-nan Zhang, and Linh V. Nguyen

Optical fiber refractive index sensor with low detection limit and large dynamic range using a hybrid fiber interferometer

Journal of Lightwave Technology, 2019; 37(13):2954-2962

© 2019 IEEE. Personal use is permitted, but republication/redistribution requires IEEE permission. See http://www.ieee.org/publications_standards/publications/rights/index.html for more information.

Published version at: <http://dx.doi.org/10.1109/JLT.2019.2908023>

PERMISSIONS

<https://www.ieee.org/publications/rights/author-posting-policy.html>

Author Posting of IEEE Copyrighted Papers Online

The IEEE Publication Services & Products Board (PSPB) last revised its Operations Manual Section 8.1.9 on Electronic Information Dissemination (known familiarly as "author posting policy") on 7 December 2012.

PSPB accepted the recommendations of an ad hoc committee, which reviewed the policy that had previously been revised in November 2010. The highlights of the current policy are as follows:

- The policy reaffirms the principle that authors are free to post their own version of their IEEE periodical or conference articles on their personal Web sites, those of their employers, or their funding agencies for the purpose of meeting public availability requirements prescribed by their funding agencies. Authors may post their version of an article as accepted for publication in an IEEE periodical or conference proceedings. Posting of the final PDF, as published by IEEE *Xplore*[®], continues to be prohibited, except for open-access journal articles supported by payment of an article processing charge (APC), whose authors may freely post the final version.
- The policy provides that IEEE periodicals will make available to each author a preprint version of that person's article that includes the Digital Object Identifier, IEEE's copyright notice, and a notice showing the article has been accepted for publication.
- The policy states that authors are allowed to post versions of their articles on approved third-party servers that are operated by not-for-profit organizations. Because IEEE policy provides that authors are free to follow public access mandates of government funding agencies, IEEE authors may follow requirements to deposit their accepted manuscripts in those government repositories.

IEEE distributes accepted versions of journal articles for author posting through the Author Gateway, now used by all journals produced by IEEE Publishing Operations. (Some journals use services from external vendors, and these journals are encouraged to adopt similar services for the convenience of authors.) Authors' versions distributed through the Author Gateway include a live link to articles in IEEE *Xplore*. Most conferences do not use the Author Gateway; authors of conference articles should feel free to post their own version of their articles as accepted for publication by an IEEE conference, with the addition of a copyright notice and a Digital Object Identifier to the version of record in IEEE *Xplore*.

1 November 2019

<http://hdl.handle.net/2440/121695>

Optical fiber refractive index sensor with low detection limit and large dynamic range using a hybrid fiber interferometer

Xuegang Li, Stephen C. Warren-Smith, Heike Ebendorff-Heidepriem, Yanan Zhang and Linh V. Nguyen.

Abstract—A refractive index (RI) fiber sensor with low detection limit but large dynamic range is proposed and demonstrated using an exposed core microstructured optical fiber. The exposed-core fiber is highly birefringent due to its asymmetry and also supports multimode propagation, thus can be used simultaneously as a Mach-Zehnder and Sagnac interferometer. The Mach-Zehnder interference is significantly more phase-sensitive to RI due to a longer effective path length difference. This leads to a lower detection limit compared to that for the Sagnac interferometer, which has a larger free spectral range (FSR) that allows the dynamic range of the RI measurement to be extended. By combining these two interferometers, the proposed sensor achieves a detection limit of as low as 6.02×10^{-6} refractive index units (RIU) while maintaining a large dynamic range from 1.3320 RIU to 1.3465 RIU. The proposed sensor also has the advantages of bio-compatibility, low cost, high stability, small size, ability to operate remotely and simple to be fabricated.

Index Terms—Refractive index sensor, Optical fiber applications, Optical sensors, Interferometers.

I. INTRODUCTION

Refractive index sensing is an important tool that can be applied to a wide variety of industrial, chemical and biological applications. This is because many physical and chemical parameters can be measured by monitoring the change of RI, such as gas concentration [1-3], humidity [4, 5], solution concentration [6], temperature [7], magnetic field [8-10], pH

Stephen C. Warren-Smith is funded by a Ramsay Fellowship provided by the University of Adelaide. This work was performed, in part, at the Optofab node of the Australian National Fabrication Facility utilizing Commonwealth and SA State Government funding. Xuegang Li gratefully acknowledges financial support from the China Scholarship Council. This work was supported in part by the Fundamental Research Funds for the Central Universities under Grant N160406004. Linh Viet Nguyen acknowledges the support of the Australian Government's Cooperative Research Centres Program. The authors acknowledge Peter Henry and Alastair Dowler for their contribution to the fiber fabrication.

Xuegang Li is with College of Information Science and Engineering, Northeastern University, Shenyang 110819, China, and also with Institute for Photonics and Advanced Sensing (IPAS) and School of Physical Sciences, The University of Adelaide, Adelaide, South Australia 5005, Australia (e-mail: lixuegang@stunmail.neu.edu.cn).

[11], biomolecules [12], and DNA [13]

In biochemistry, RI based sensing offers a pathway to avoid the conventional method that utilizes fluorescence labelling for detection. Functionalization with fluorescent tags is typically complex and expensive and the technique suffers from photo-bleaching of organic fluorophores [14]. In order to simplify preparation procedures, achieve high sensitivity, and avoid the high cost and photo-bleaching of fluorescent tags, optical fiber RI-based biosensors have been studied extensively [15, 16] as the optical fiber platform offers a number of advantages, namely small size, bio-compatibility, immunity to electromagnetic interference, and the potential for remote operation. There are numerous optical fiber sensing mechanisms that have been demonstrated for use as RI sensors, with examples including Mach-Zehnder (MZ) interferometers [12, 17-21], Fabry-Perot interferometers [22, 23], surface plasmon resonance [24, 25], fiber Bragg-gratings [26-28], long-period fiber gratings [29-31], and Sagnac (SG) interferometers [13, 32]. There are typically trade-offs in performance depending on the mechanism used. For example, fiber Bragg gratings and long period gratings offer the ability to measure RI, but suffer from low sensitivity [26-29]. On the other hand, surface plasmon resonance based sensors offer sensitive measurement of RI, but at the expense of high optical loss and the potential instability of thin metal films [6, 24, 25].

Interferometric RI sensing techniques, such as Mach-Zehnder [12, 21], Fabry-Perot cavity [23] and Sagnac [13, 32] interferometers, as well as whispering gallery mode resonators [33, 34], can offer very high sensitivity. For example, in [21, 23, 32] the RI sensitivities of proposed Mach-Zehnder, Fabry-Perot and Sagnac interferometers are 1.01×10^4 , 3.09×10^4 , and

Stephen C. Warren-Smith and Heike Ebendorff-Heidepriem are with Institute for Photonics and Advanced Sensing (IPAS) and School of Physical Sciences, The University of Adelaide, Adelaide, South Australia 5005, Australia, and also with ARC Centre of Excellence for Nanoscale BioPhotonics (CNBP), The University of Adelaide, Adelaide, South Australia 5005, Australia (e-mail: heike.ebendorff@adelaide.edu.au, stephen.warrensmith@adelaide.edu.au).

Yanan Zhang is with College of Information Science and Engineering, Northeastern University, Shenyang 110819, China. (zhangyanan@ise.neu.edu.cn)

Linh V. Nguyen is with Institute for Photonics and Advanced Sensing (IPAS) and School of Physical Sciences, The University of Adelaide, Adelaide, South Australia 5005, Australia, and also with Plant Biosecurity Cooperative Research Centre, Bruce, Canberra 2617, ACT, Australia (e-mail: linhnguyen.research@gmail.com).

> REPLACE THIS LINE WITH YOUR PAPER IDENTIFICATION NUMBER (DOUBLE-CLICK HERE TO EDIT) < 2

1.25×10^4 nm/RIU, respectively. However, such sensors require complicated device fabrication processes, such as micro/nano-machining of channels [23] and optical resonators [34]. They also have fragility issues, as they are made from fiber tapers [13, 32]. Above all, these types of sensors often have a trade-off between sensitivity and measurement dynamic range due to the periodicity of interference spectra. If the RI changes too significantly between spectral scans, there will be an unaccounted 2π phase shift. This leads to a trade-off between sensitivity and dynamic range. As an example, in [32] Y. Han *et al.* proposed a single-mode micro-fiber Sagnac loop interferometer based on single-mode micro-fiber, which exhibited relatively a high sensitivity to the RI of 1.25×10^4 nm/RIU, but with a relatively small dynamic range of only 4.8×10^{-4} RIU.

In principle, the dynamic range of traditional interferometric techniques can be increased by accounting for 2π phase shifts by continuously measuring RI. However, correcting for the 2π phase shift is only possible if the biochemical-binding event happens in a slower period than the signal acquisition time, leaving out the potential use in monitoring fast binding biochemical events. In addition, in some remote measurements, such as ocean monitoring, RI sensors are required to work for long periods and thus continuous monitoring may not be possible, but long-term changes in RI may be larger than the small dynamic range.

Recently, Chen *et al.* demonstrated a dual-cavity Fabry–Perot interferometer formed by cleaved single mode fiber and a small refractive-index-modified defect in the fiber core to achieve both high sensitivity and a large dynamic range [35]. However, the proposed sensor is an intensity modulated fiber-optic sensor, which is subject to influence from vibration, light source fluctuations and end-face contamination.

In our previous work, we achieved a high sensitivity refractive index sensor using the exposed-core microstructured optical fiber Mach-Zehnder interferometer with a simple fabrication process that overcomes the fragility issues associated with traditional micro-fibers [12]. However, the sensor still has a relatively small dynamic range of 2.1×10^{-3} RIU. We also achieved a high wavelength sensitivity and relatively large dynamic range biosensor using a Sagnac-interferometer [36]. However, this sensor has a higher detection limit (DL) compared with [12].

In this paper, we demonstrate a method to combine the two interferometric modalities, a Mach-Zehnder interferometer and a Sagnac loop interferometer, in a single optical fiber sensing platform to realize a high sensitivity, low detection limit and wide-dynamic range RI sensor. Our proposed approach combines the relatively high sensitivity and low detection limit of the Mach-Zehnder interferometer with the relatively large dynamic range of the Sagnac interferometer in a unified sensor structure that is simple and cost-effective.

II. OPERATING PRINCIPLE

A. Hybrid interferometer based on exposed microstructured optical fiber

Fig. 1 (a) shows a schematic diagram of the proposed hybrid interferometer based on the exposed-core fiber (ECF). ECF is a microstructured optical fiber with two enclosed air holes and an open side, which allows external liquid to directly access to evanescent field, as shown in Fig. 1 (b). The sensor was fabricated by splicing a section of ECF between two single mode fibers (SMFs) in a Sagnac loop, forming a hybrid Mach-Zehnder/Sagnac interferometer. The ECF was packaged within a flow cell to measure different RI liquids. The asymmetry of the fiber core creates an optical birefringence, leading to Sagnac interference (Sagnac interferometer), while the high numerical aperture of ECF allows for propagation of a number of higher order modes, creating interference patterns between different modes (Mach-Zehnder interferometer).

The operation principle of the proposed sensor is as follows: Light from a broad-band source is split into clockwise and counterclockwise beams via a 3 dB coupler as it enters the loop, as shown in Fig. 1 (a). A net phase difference is accumulated as the two polarization fundamental modes (red and purple lines in Figs. 1 (a) and (c)) through the length of the birefringent ECF, leading to Sagnac interference when the clockwise and counterclockwise beams are recombined at the 3 dB coupler [8]. Meanwhile, when the light enters the ECF from the lead-in SMF, higher order modes (black lines in Fig. 1 (c)) are excited and propagate along the ECF core. At the ECF/SMF splicing point, the higher order modes of the ECF are coupled into the

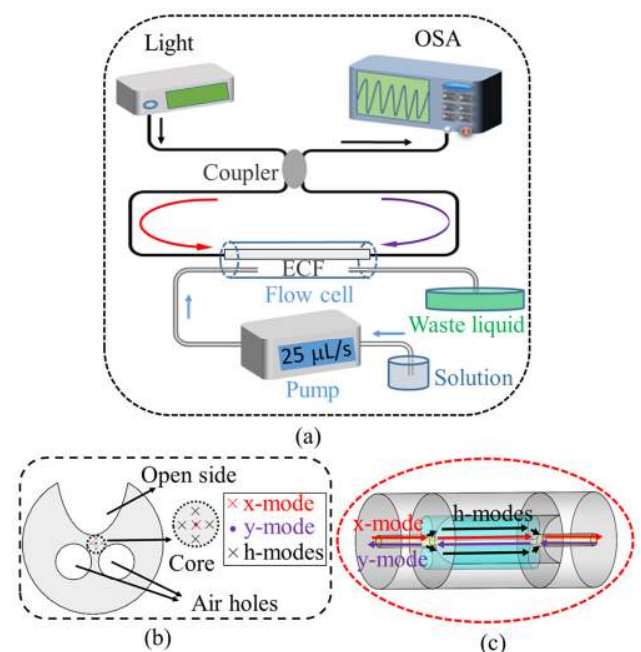


Fig. 1 (a) Schematic diagram and experimental setup of the proposed sensor system. (b) Schematic cross section of the ECF. (c) Schematic diagram of the Sagnac interferometer and Mach-Zehnder interferometer: red line refers to the x-polarized fundamental mode, purple line refers to the y-polarized fundamental mode and black lines refer to the higher order (h) modes.

> REPLACE THIS LINE WITH YOUR PAPER IDENTIFICATION NUMBER (DOUBLE-CLICK HERE TO EDIT) < 3

core of the SMF and the Mach-Zehnder interference occurs between the different order modes due to different propagation constants. A hybrid interference pattern composed of both Mach-Zehnder and Sagnac interferences is then formed in the transmission spectrum of the structure.

For both interferences types the interference spectrum can be modelled by a simple two-mode interference equation,

$$I_{out} = I_1 + I_2 + 2\sqrt{I_1 I_2} \cos \varphi, \quad (1)$$

where I_1 and I_2 are light intensities of two different modes, and φ is the phase difference between them. For the Sagnac interference, the interference occurs between x-polarization and y-polarization fundamental modes. In this case, I_1 and I_2 are light intensities of x-polarization and y-polarization fundamental modes and the phase of the Sagnac interference, φ_{SG} , can be expressed as,

$$\varphi_{SG} = \frac{2\pi L}{\lambda} B, \quad (2)$$

where λ is the free space wavelength, L is the length of the ECF, and B is the birefringence of the ECF and is defined as the difference between the effective indices of the x-polarization and y-polarization fundamental modes. Note that the higher order modes are typically more weakly excited compared with the fundamental mode and thus the birefringence effect on higher order modes can be ignored.

Due to the high numerical aperture of the ECF, it is a multimode fiber. The number of modes in an optical fiber can be estimated by calculating the normalized frequency using a step-index optical fiber model, so-called V-parameter, which is described as:

$$V = \frac{2\pi a}{\lambda} \sqrt{n_1^2 - n_2^2}, \quad (3)$$

where n_1 and n_2 are the refractive indices of the core and cladding, respectively, and a is the radius of the core. For the exposed-core fiber, $a = 3.75$, $n_2 = 1$, and $n_1 = 1.4469$ when the wavelength of operation is 1300 nm. This gives a value of $V = 18.94$. The number of modes, M , that can be guided by the ECF is estimated to be 145 using the approximation $M = 4V^2/\pi^2$.

Note that M is an estimated value as the ECF is not a standard step index fiber. However, only a few modes are involved in the interferometer as only a few modes are coupled via the spliced SMF, as detailed in our previous work [12]. For the Mach-Zehnder interference, the interference might occur between any two different higher order modes. Thus, the Mach-Zehnder interference spectrum is the superposition of several individual interferences. However, the individual Mach-Zehnder interference patterns can be de-multiplexed using fast Fourier transform (FFT), allowing for analysis of each constituent interference pattern. In this case, the phase for a specific pair of propagation modes $\{i,j\}$ forming an interference can be expressed as,

$$\varphi_{MZ} = \frac{2\pi L}{\lambda} \Delta n_{eff}, \quad (4)$$

where $\Delta n_{eff} = n_i - n_j$ is the effective index difference between the i -order and j -order modes. The free spectral range (FSR) is the wavelength spacing between two adjacent minima/maxima. For Sagnac and Mach-Zehnder interferences, FSRs can be expressed as,

$$FSR_{SG} = \frac{\lambda^2}{BL}, \quad (5)$$

and

$$FSR_{MZ} = \frac{\lambda^2}{\Delta n_{eff} L}. \quad (6)$$

From (2) and (4), we can get the phase of Sagnac and Mach-Zehnder interferences respectively change with the change of B and Δn_{eff} , which are functions of external RI, n_{ext} . For a fixed length L of the fiber, with a change in the external RI, the changes in phase, $\Delta\varphi_{SG}$ and $\Delta\varphi_{MZ}$, of two interferences caused by the change of B and Δn_{eff} can be respectively expressed as,

$$\Delta\varphi_{SG} = \frac{2\pi L}{\lambda} \Delta B, \quad (7)$$

and

$$\Delta\varphi_{MZ} = \frac{2\pi L}{\lambda} \Delta(\Delta n_{eff}). \quad (8)$$

Thus, the transmission spectrum of the structure is the result of superimposing Sagnac interference and Mach-Zehnder interference. The phase (φ_{SG} or φ_{MZ}) associated with each interference pattern formed by a pair of modes can be obtained by first applying an FFT on the transmission spectra. Each interference pattern shows a peak in the FFT. For each peak, the value of the phase is taken from the complex value of the FFT peak associated with an interference pattern in the FFT spectrum. The value of phase will change with respect to changes in the ambient medium and thus can be independently tracked. FFT techniques are widely used for de-multiplexing interference spectra [12, 36, 37]. Not only can this technique be used for de-multiplexing interference spectra, but has been shown to be more precise than other methods of tracking interference spectrum shifts, such as peak tracking or function fitting [38].

B. Mode distribution of the exposed-core microstructured optical fiber

In order to understand the mode distribution of the ECF and the resulting sensitivity, the structure was investigated using a finite-element method (COMSOL v5.2). The simulation geometry was imported from a scanning electron microscope (SEM) image of the ECF, as shown in Fig.2 (a). The core and cladding diameters of the ECF were 7.5 μm and 160 μm , respectively. Fig. 2 (b) shows the geometry of the theoretical model, where blue represents air, grey represents the silica core of the ECF, and green represents the exposed side for sensing.

> REPLACE THIS LINE WITH YOUR PAPER IDENTIFICATION NUMBER (DOUBLE-CLICK HERE TO EDIT) <

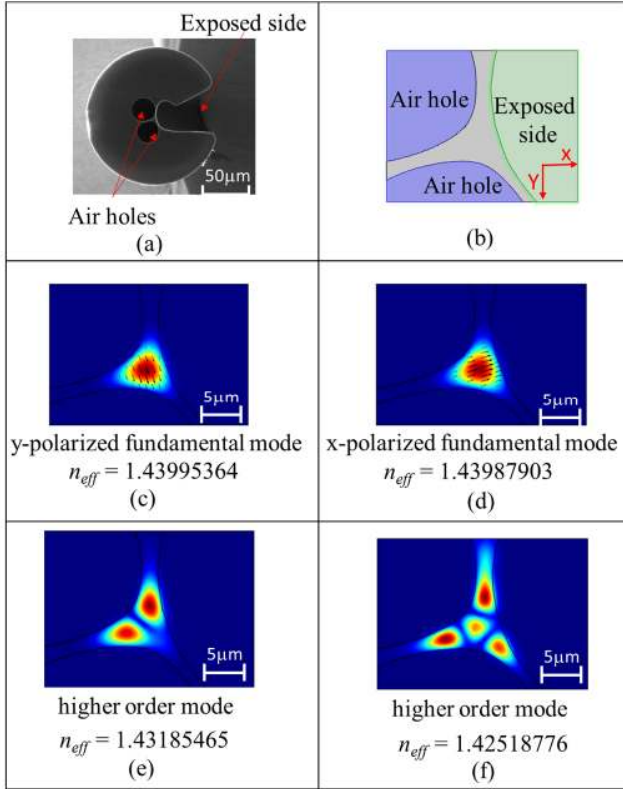


Fig. 2. Effective mode indices and norm of the electric fields of the first three modes in the core region with $\lambda = 1.30 \mu\text{m}$. (a) A scanning electron microscope (SEM) image of the ECF. (b) Geometry of the theoretical model, blue represents air, grey represents the silica core of the ECF and green represents the exposed side for sensing. (c), (d), (e) and (f) are the simulated electric field distributions of the x-polarized fundamental mode, y-polarized fundamental mode and two example higher order modes when the exposed side was set as water, respectively.

The refractive index of the silica core was defined by the standard Sellmeier equation for fused silica glass. At a wavelength of 1300 nm the refractive index of the ECF is 1.4469. In our simulation, the exposed side was set as water, with RI of 1.332. Figs. 2 (b) and (c) are the simulated distributions for the x-polarized and y-polarized fundamental modes, respectively, at a wavelength, λ , of 1.30 μm . From the effective index of the modes shown in Figs. 2 (c) and (d) it can be seen that there is a phase birefringence of $B = |n_{eff}^x - n_{eff}^y| = 7.461 \times 10^{-5}$ at $\lambda = 1.30 \mu\text{m}$ in the ECF. This phase birefringence allows the ECF to be used within a Sagnac interferometer.

Depicted in Figs. 2 (e) and (f) are two examples of higher order modes that can propagate within the core of the ECF. From Figs. 2 (c), (d), (e) and (f) we can see that there are effective index differences between different order modes, for example, the effective index difference between the modes shown in Figs. 2 (c) and (e) is $\Delta n_{eff}^1 = 8.099 \times 10^{-3}$ and between the modes in Figs. 2 (d) and (e) is $\Delta n_{eff}^2 = 8.024 \times 10^{-3}$. These effective index differences allow the ECF to be used as a Mach-Zehnder modal interferometer. The values of Δn_{eff}^1 and Δn_{eff}^2 are much higher than B , making the free spectral ranges of the Mach-

Zehnder interferences much smaller than that for the Sagnac interference (see (5) and (6)).

C. Numerically predicted refractive index sensitivity

The numerical model was utilized to determine the sensitivity of the ECF to RI variations when in either a Sagnac or Mach-Zehnder interferometer configuration. This was implemented by changing the RI of the sensing-liquid, which was filled in the exposed side of Fig. 2 (b). Fig. 3 (a) shows a linear relationship between birefringence of the ECF at $\lambda = 1.30 \mu\text{m}$ and external RI. It can be seen that the birefringence of the ECF increases with external RI.

The Mach-Zehnder interferences mainly occur between low-order modes, for example, x-fundamental mode and the second order mode (Fig. 2 (e)), and y-fundamental mode and the second order mode. However, the difference between Δn_{eff}^1 and Δn_{eff}^2 (7.5×10^{-5}) is relatively small compared to their value. Therefore these two interferences are essentially identical, that is, similar free spectral range and sensitivity to external RI. The effective index difference between the x-fundamental mode and the higher order mode shown in Fig. 2 (e) with different external

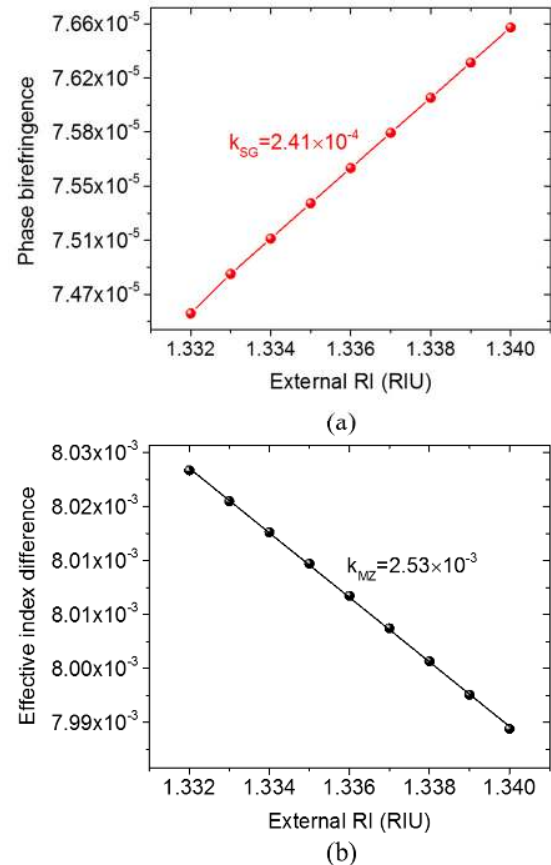


Fig. 3 (a) Phase birefringence, B , with different external RI and (b) the effective index difference between the x-fundamental mode and a higher order mode in Fig. 2 (e), Δn_{eff} , with different external RI, with $\lambda = 1.30 \mu\text{m}$.

> REPLACE THIS LINE WITH YOUR PAPER IDENTIFICATION NUMBER (DOUBLE-CLICK HERE TO EDIT) <

RI is shown in Fig. 3 (b), which shows that increasing the external RI leads to a decrease in Δn_{eff} . The different modes have different proportions of optical field in the exposed core, thus leading to a smaller Δn_{eff} when the external RI is increased [36]. The change of the external RI with both B and Δn_{eff} of the fiber leads to phase changes for both the Sagnac spectra and Mach-Zehnder spectra.

According Fig. 3 (a), the change of B (ΔB) can be expressed as, $\Delta B = k_{SG} \Delta n_{ext}$, where Δn_{ext} is the change of the external RI and k_{SG} is the slope in Fig. 3 (a). Combining with (7), the phase sensitivity of the Sagnac interference spectrum can be expressed as,

$$S_{SG} = \Delta \varphi_{SG} / \Delta n_{ext} = k_{SG} \frac{2\pi L}{\lambda}. \quad (9)$$

For a 20 cm ECF sensor, the phase sensitivity of the Sagnac interference spectrum to external RI is 233 rad/RIU by using (9). Similarly, the phase sensitivity of the Mach-Zehnder interference spectrum can be expressed as,

$$S_{MZ} = \Delta \varphi_{MZ} / \Delta n_{ext} = k_{MZ} \frac{2\pi L}{\lambda}, \quad (10)$$

where k_{MZ} is the slope in Fig. 3 (b). Using this equation, the phase sensitivity of the Mach-Zehnder interference spectrum to external RI is -2,446 rad/RIU. For a 2π period, the RI measurement range of the Sagnac and Mach-Zehnder interferometers are 0.0270 RIU and 0.00257 RIU, respectively.

It can be concluded that the Mach-Zehnder interferometer has a higher phase sensitivity but a narrower dynamic range, while the Sagnac interferometer has a larger dynamic range but suffers from a lower phase sensitivity. Thus, if we monitor phase change of the Sagnac and Mach-Zehnder interference at the same time, the co-existence of high sensitivity and a large dynamic range can be achieved.

III. EXPERIMENTAL RESULTS

A. Fabrication and transmission characterization

Exposed-core fiber was fabricated as previously described [28, 39]. Briefly, three 2.8 mm holes were ultrasonically drilled into the centre of a 20 mm fused silica glass rod. A 1 mm slot was then cut from one hole to the surface, which forms the open slot seen in Fig. 2(a). The preform was then drawn to 160 μm outer diameter fiber using a 6 m draw tower at approximately 2000°C, using positive pressure to inflate the two closed holes. A 20 cm length of ECF was fusion-spliced into a fiber loop mirror using the same splicing conditions previously reported [28]. Briefly, the ECF was spliced to conventional single mode fiber (SMF28e) using an arc splicer (Fujikura FSM-100P). Standard splicing parameters were used, except slightly lower arc power, increased arc duration, and manual core alignment.

Light from a broad-band supercontinuum source (NKT Photonics SuperK Extreme) was split into two beams (clockwise and counterclockwise) via a 3 dB coupler and the

two beams were recombined at the 3 dB coupler, leading to a Sagnac interference spectrum. Meanwhile, the Mach-Zehnder interference occurred between the different modes of the ECF due to the SMF-ECF-SMF structure. The resulting combined interference spectrum was then measured by using an optical spectrum analyzer (OSA, Ando-6315E) with a resolution of 0.05 nm, as shown in Fig. 4 (a). It should be noted that the Mach-Zehnder interference is much weaker than the Sagnac interference because the higher order modes are typically weakly excited.

Fig. 4 (b) shows the FFT spectrum of the combined interference spectrum shown in Fig. 4 (a). In our paper, FFT is performed on the spectrum with a linear y-axis and the mean value has been removed. The main peak (Peak 1) at 0.00999 nm^{-1} in the FFT spectrum corresponds to the Sagnac interference, while two lower peaks, Peak 2 at 0.699 nm^{-1} and Peak 3 at 0.759 nm^{-1} , represent two Mach-Zehnder interferences. According Fig. 2, the effective index difference between the x-fundamental mode and the higher order mode is smaller than the difference between the y-fundamental mode and the higher order mode. As a smaller effective index

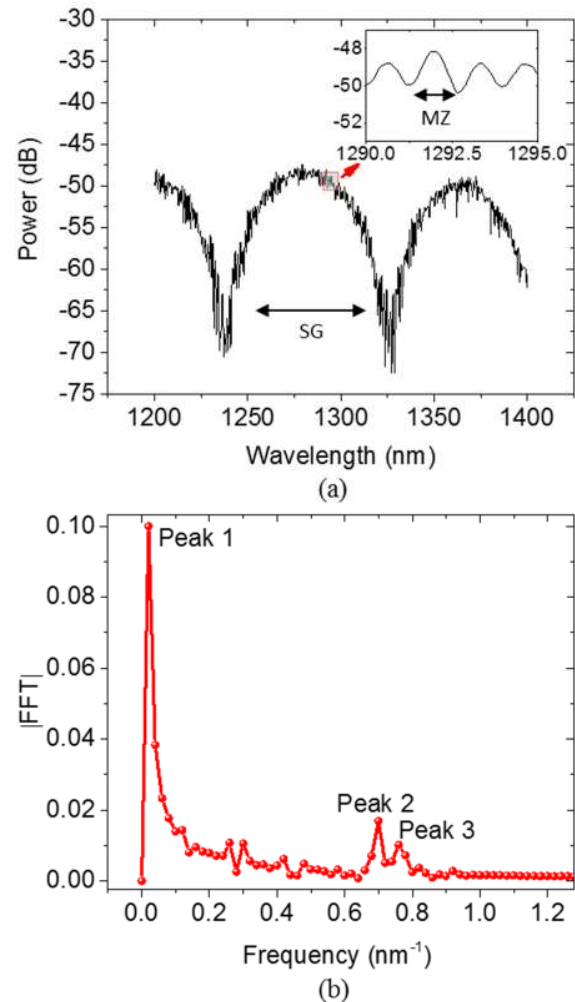


Fig. 4 (a) Transmission spectrum of the sensor in deionized water and (b) FFT of the spectrum in (a). SG indicates the Sagnac interference spectrum with low-frequency interference. MZ (inset) shows the high-frequency Mach-Zehnder interference.

> REPLACE THIS LINE WITH YOUR PAPER IDENTIFICATION NUMBER (DOUBLE-CLICK HERE TO EDIT) < 6

difference leads to a larger FSR, Peak 2 therefore represents the interference between the x-fundamental mode and the higher order mode, and Peak 3 represents the interference between y-fundamental mode and the higher order mode. In our paper, Peak 2 was used selected as the Mach-Zehnder interference sensing peak. Considering (5) and (6), we determine that B is 8.442×10^{-5} and Δn_{eff} is 5.907×10^{-3} , which are close to the theoretical values of 7.461×10^{-5} and 8.024×10^{-3} .

B. Refractive index sensing

The experiment setup for RI sensing is shown in Fig.1 (a). The ECF was placed into a silica capillary flow cell (inner diameter of 650 μm). External RI was changed by flowing NaCl solutions of different concentration through the flow cell via a pump (LongerPump BT100-1F). All experiments were operated in a temperature controlled laboratory to avoid the influence of temperature. Spectra were recorded while different concentrations (0-1% with 0.1% steps) of sodium chloride in

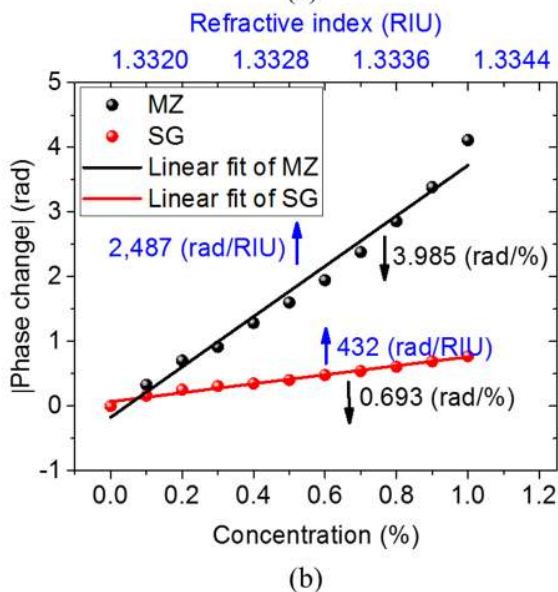
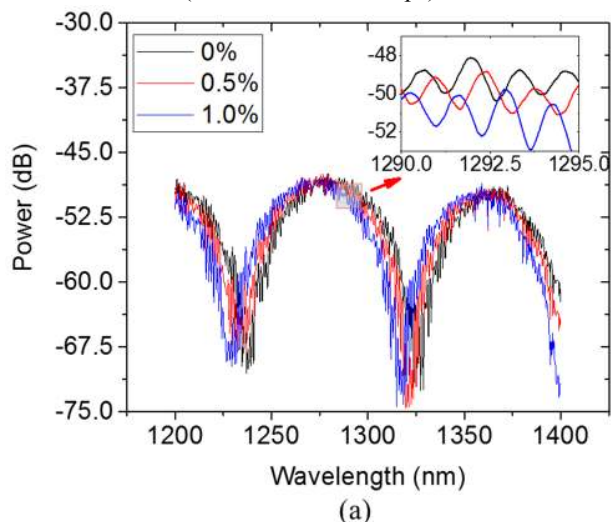


Fig. 5 (a) Spectra of the proposed platform subjected to the different NaCl concentrations and (b) the absolute phase change, $|\Delta\phi|$, at the frequency of 0.0099 nm^{-1} corresponding to the Sagnac interference, and 0.689 nm^{-1} representing the primary Mach-Zehnder interference.

deionized water solutions were passed through the flow-cell, with three example spectra shown in Fig. 5 (a). Fig. 5 shows that the Sagnac interference spectra shifted to shorter wavelengths with increasing concentration, while the Mach-Zehnder interference spectra shifted to longer wavelengths with increasing concentration. The absolute phase change with respect to concentration was monitored for both the Sagnac and Mach-Zehnder interferences via the fast Fourier transform of the spectra, as shown in Fig. 5 (b).

We set the phase of the first spectrum, with 0% NaCl concentration, as the original phase. The phase change ($\Delta\phi$) for different NaCl concentrations relative to the original phase value is obtained by subtracting the value of the original phase. The phase sensitivities of the Sagnac interference and Mach-Zehnder interference to concentration are $0.693 \text{ rad}/\%$ and $3.985 \text{ rad}/\%$, respectively. Converting to RI sensitivities [40], the sensitivities are estimated to be $432 \text{ rad}/\text{RIU}$ and $2,487 \text{ rad}/\text{RIU}$, respectively. This compares to the theoretical values of $233 \text{ rad}/\text{RIU}$ and $2,446 \text{ rad}/\text{RIU}$, respectively. The difference can be caused by errors associated with light source and detector stability, recording and importing the exposed-core fiber image for numerical modelling, and the NaCl solutions [36]. For a 2π period, the RI measurement range of the Sagnac and Mach-Zehnder interferometers are 0.0145 RIU and 0.00253 RIU , respectively.

C. Detection limit and measurement range

Detection limit (DL) is the minimum concentration or minimum amount of analyte in a sample that can be reliably distinguished from zero. It is a critical parameter to evaluate the performance of the sensor. It can be deduced by taking into account the noise in the transduction signal [41]. We use the definition of DL as [42]:

$$DL = 3.3\sigma / S, \quad (11)$$

where σ is the standard deviation of the response and S is the slope of the calibration curve. The standard deviation of the response can be obtained by measuring the standard deviation of the blank response. In our case, the blank response was obtained when the sensor was immersed in pure water.

To get the blank responses and determine the DLs for the two interferometer modes the exposed-core fiber was immersed into pure water for 30 min and the spectrum for each was recorded every two minutes. The phase changes at different times were obtained by subtracting the average phase from the real-time phase and are presented in Fig. 6, which shows the blank responses of the two sensing schemes.

The phase changes in Fig. 6 are due to the experimental conditions in the laboratory (temperature fluctuation, flow rate of the sensor) and stability of the light source and detector. The standard deviation, σ_1 , of the Sagnac interference was measured to be 0.00186 rad and the standard deviation, σ_2 , of Mach Zehnder interference was 0.00454 rad . Using the standard deviations from the data in Fig. 6 and the phase sensitivities from Fig. 5 (b), the DLs were determined using (11) and are shown in Table 1. The results show that the Mach Zehnder interferometer, which has the higher phase sensitivity to RI, indeed offers a lower detection limit compared to the Sagnac interferometer.

> REPLACE THIS LINE WITH YOUR PAPER IDENTIFICATION NUMBER (DOUBLE-CLICK HERE TO EDIT) < 7

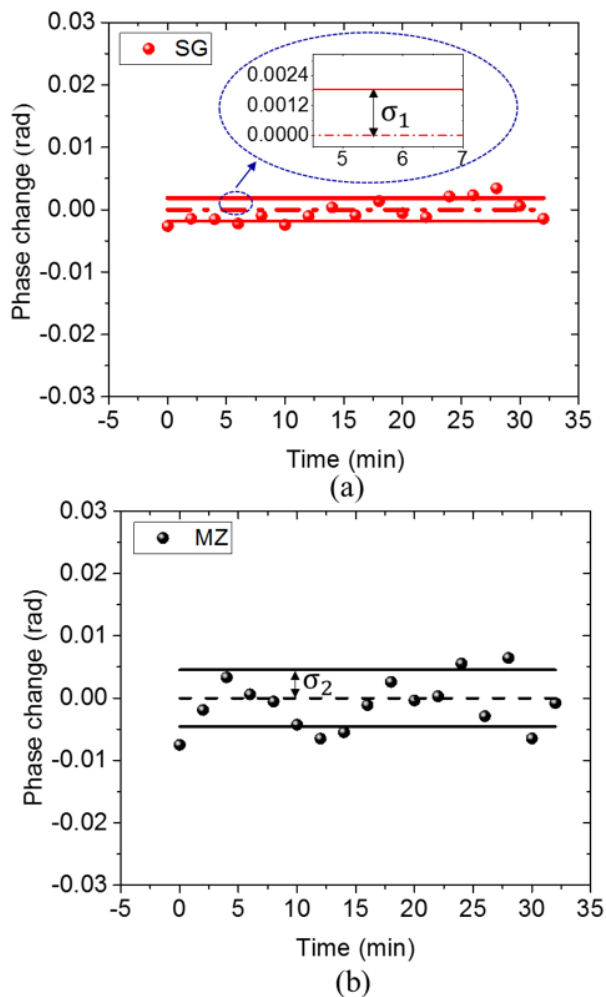


Fig. 6. The phase change of the sensor by immersing the ECF into water for 30 min. (a) Sagnac interferometer. (b) Mach-Zehnder interferometer. The red and black lines represent one standard deviation over the measurement duration.

TABLE 1
INDEXES OF THE SAGNAC AND MACH-ZEHNDER INTERFEROMETER

Type	Standard deviation of $\Delta\varphi$ (rad)	Concentration DL (%)	RI DL (RIU)	Dynamic range (RIU)
Sagnac interferometer	0.00186	0.00886	1.42×10^{-5}	0.0145
Mach-Zehnder interferometer	0.00454	0.00376	6.02×10^{-6}	0.0025

To demonstrate the ability to measure small concentrations, the ECF sensor was immersed in small concentrations of sodium chloride solution, as shown in Fig. 7. Figs. 7 (a) and (b) are the phase changes of the Mach-Zehnder interference spectra and Sagnac interference spectra with different concentrations, respectively. Fig. 7 shows that the Mach-Zehnder interferometer has a better ability to resolve low concentrations compared with Sagnac interferometer, such as the concentration of 0.0125% ($\Delta RI = 2.00 \times 10^{-5}$ RIU) or 0.025% ($\Delta RI = 4.00 \times 10^{-5}$ RIU).

However, as previously discussed, the Mach-Zehnder

interferometer has a smaller dynamic range than the Sagnac interferometer. Fig. 8 shows the absolute phase changes of the Sagnac interference spectrum and Mach-Zehnder interference spectrum by immersing the ECF into different concentrations in the range of 0-8%. For the Mach-Zehnder interferometer, large external RI change leads to an unaccounted 2π phase shift, as shown in Fig. 8 (b). The black dash line is the adjusted absolute phase change of the Mach-Zehnder interference by adding $2k\pi$, where k is an integer. Fig. 8 shows that the dynamic range of Sagnac interferometer is almost six times more than the Mach-Zehnder interferometer. Therefore, we can achieve a low DL and large dynamic range by simultaneously monitoring both interferometers due to the simultaneous existence of both interferences in a single optical fiber sensing platform.

The sensor can achieve accurate measurement when the RI value is over the measuring RI range of the Mach-Zehnder interferometer by first determining the RI value via Sagnac interferometer and then further accurately measuring via the Mach-Zehnder interferometer. For example, if we measure a solution with 5.0% sodium chloride, it cannot be measured via

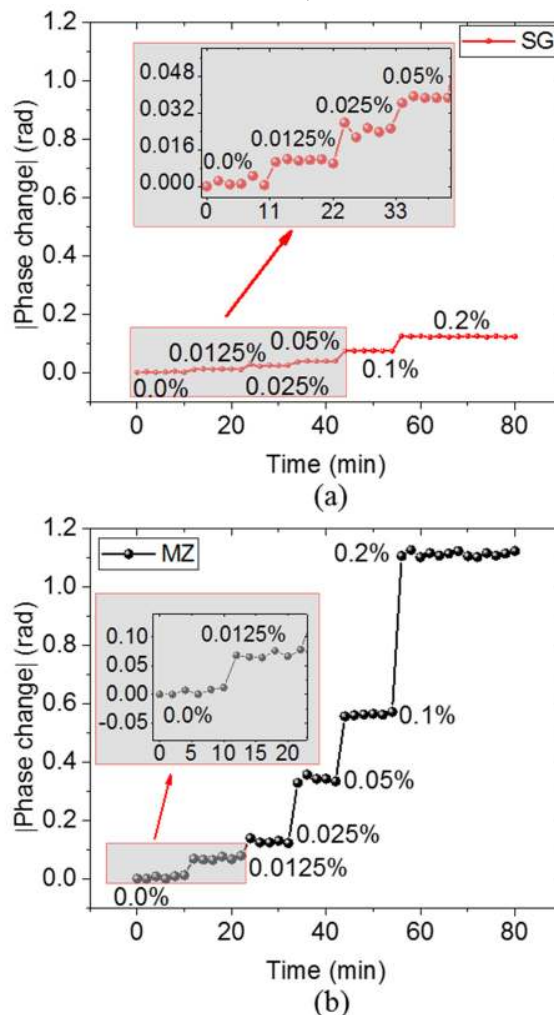


Fig. 7. Absolute phase changes of the sensor with subtle change in the concentration of sodium chloride. (a) Absolute phase change of the Sagnac interference spectrum. (b) Absolute phase change of the Mach-Zehnder interference spectrum.

a single Mach-Zehnder interferometer because the phase change is over 2π and there are several concentrations corresponding to this phase value, as shown by the blue dash line in Fig. 8 (b). However, we can first determine the concentration via the Sagnac interferometer, which gives, in this example, a value of $5.0\% \pm 0.00268\%$, where the error is obtained by dividing the standard deviation by the sensitivity of the Sagnac interferometer, that is, $\sigma/S = 0.00268\%$. We can then accurately measure the concentration via the phase change of Mach-Zehnder interferometer plus $2k\pi$. In this example, the value of $k = 2$ is obtained via the Sagnac interferometer, yielding a final measurement of concentration to be a more precise value of $5.0\% \pm 0.00114\%$.

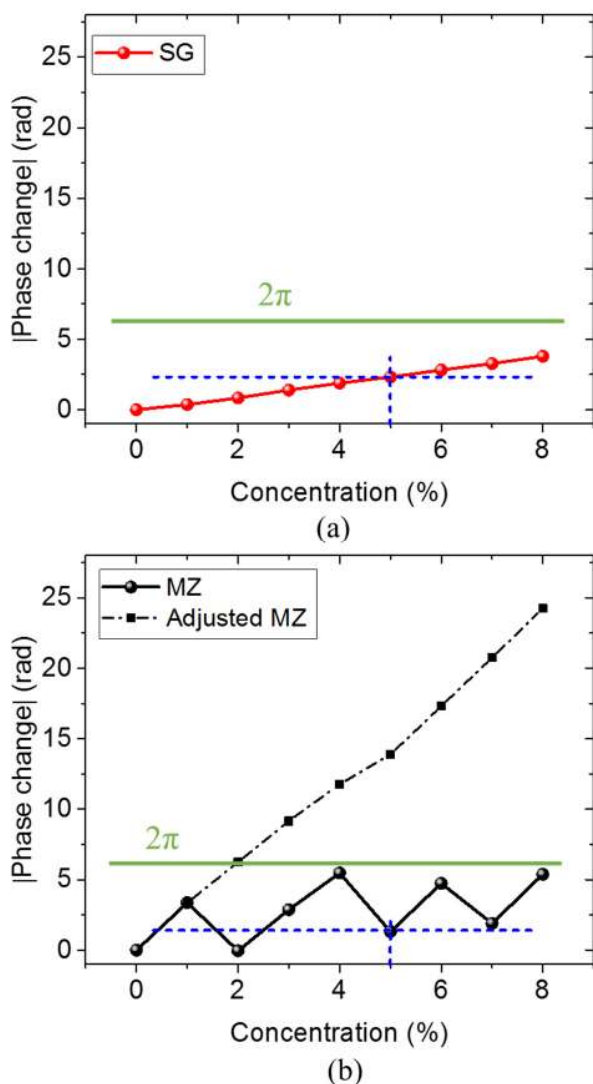


Fig. 8. Absolute phase changes of the (a) Sagnac interference spectrum and (b) Mach-Zehnder interference spectrum by immersing the ECF into the different concentrations (0%~8% with a 1% step). The blue dash line is the phase values for the example of a 5% concentration of sodium chloride.

IV. CONCLUSION

A high-sensitivity, low-DL, large dynamic range RI sensor combining Sagnac and Mach-Zehnder interferences has been

proposed and experimentally demonstrated for the first time in a single exposed-core microstructured optical fiber. It was achieved by combining the high sensitivity and low detection limit of the Mach-Zehnder interferometer with the large dynamic range of the Sagnac interferometer. The theoretical and experimental analysis shows that the sensor could resolve the problem of trade-off between high sensitivities, high detection limit and large dynamic range present in most interferometric RI sensors. The experimental results demonstrate that the proposed sensor has a high RI sensitivity of up to 2,487 rad/RIU, a low RI detection limit of 6.02×10^{-6} RIU, while maintaining a relatively large dynamic range from 1.3320 RIU to 1.3465 RIU.

The proposed sensor is particularly useful for applications where the sensing event occurs faster than the sensor acquisition time or the long-term changes in external RI larger than the small dynamic range. This could be fast biochemical-binding events or remote measurements, such as ocean monitoring, where sensors are required to work for long periods with minimal power consumption. Other merits of the proposed sensor includes bio-compatibility, small size, low cost, and is more robust, stable and simple to fabricate compared to tapered micro-fibers.

REFERENCES

- [1] Y. Zhao, Q. L. Wu, and Y. N. Zhang, "High-Sensitive Hydrogen Sensor Based on Photonic Crystal Fiber Model Interferometer," *IEEE Transactions on Instrumentation and Measurement*, vol. 66, no. 8, pp. 2198-2203, Aug, 2017.
- [2] T. Allsop, R. Neal, E. M. Davies, C. Mou, P. Bond, S. Rehman, K. Kalli, D. J. Webb, P. Calverhouse, and I. Bennion, "Low refractive index gas sensing using a surface plasmon resonance fibre device," *Measurement Science and Technology*, vol. 21, no. 9, pp. 094029, Jul, 2010.
- [3] S. Corbellini, M. Parvis, S. Grassini, L. Benussi, S. Bianco, S. Colafranceschi, and D. Piccolo, "Modified POF sensor for gaseous hydrogen fluoride monitoring in the presence of ionizing radiations," *IEEE Transactions on Instrumentation and Measurement*, vol. 61, no. 5, pp. 1201-1208, Dec, 2012.
- [4] P. J. Thomas, and J. O. Hellevang, "A fully distributed fibre optic sensor for relative humidity measurements," *Sensors and Actuators B-Chemical*, vol. 247, pp. 284-289, Aug, 2017.
- [5] X. F. Wang, G. Farrell, E. Lewis, K. Tian, L. B. Yuan, and P. F. Wang, "A Humidity Sensor Based on a Singlemode-Side Polished Multimode-Singlemode Optical Fibre Structure Coated with Gelatin," *Journal of Lightwave Technology*, vol. 35, no. 18, pp. 4087-4094, Sep, 2017.
- [6] Y. Zhao, Z. Q. Deng, and Q. Wang, "Fiber optic SPR sensor for liquid concentration measurement," *Sensors and Actuators B-Chemical*, vol. 192, pp. 229-233, Mar, 2014.
- [7] Y. Zhao, Z.-Q. Deng, and H.-F. Hu, "Fiber-optic SPR sensor for temperature measurement," *IEEE Transactions on Instrumentation and Measurement*, vol. 64, no. 11, pp. 3099-3104, Jun, 2015.
- [8] M. Deng, C. Huang, D. Liu, W. Jin, and T. Zhu, "All fiber magnetic field sensor with Ferrofluid-filled tapered microstructured optical fiber interferometer," *Optics Express*, vol. 23, no. 16, pp. 20668-74, Aug, 2015.
- [9] X.-G. Li, Y. Zhao, L. Cai, and X. Zhou, "Measurement of magnetic field and temperature based on fiber-optic composite interferometer," *IEEE Transactions on Instrumentation and Measurement*, vol. 66, no. 7, pp. 1906-1911, Jul, 2017.
- [10] Y. Zhao, R.-Q. Lv, D. Wang, and Q. Wang, "Fiber optic Fabry-Perot magnetic field sensor with temperature compensation using a fiber Bragg grating," *IEEE Transactions on Instrumentation and Measurement*, vol. 63, no. 9, pp. 2210-2214, May, 2014.
- [11] P. Hu, X. Dong, W. C. Wong, L. H. Chen, K. Ni, and C. C. Chan, "Photonic crystal fiber interferometric pH sensor based on polyvinyl alcohol/polyacrylic acid hydrogel coating," *Applied Optics*, vol. 54, no. 10, pp. 2647-52, Apr, 2015.

> REPLACE THIS LINE WITH YOUR PAPER IDENTIFICATION NUMBER (DOUBLE-CLICK HERE TO EDIT) < 9

- [12] L. V. Nguyen, K. Hill, S. Warren-Smith, and T. Monro, "Interferometric-type optical biosensor based on exposed core microstructured optical fiber," *Sensors and Actuators B-Chemical*, vol. 221, pp. 320-327, Dec, 2015.
- [13] S. Gao, L. P. Sun, J. Li, L. Jin, Y. Ran, Y. Y. Huang, and B. O. Guan, "High-sensitivity DNA biosensor based on microfiber Sagnac interferometer," *Optics Express*, vol. 25, no. 12, pp. 13305-13313, Jun, 2017.
- [14] E. Heydari, J. Buller, E. Wischerhoff, A. Laschewsky, S. Doring, and J. Stumpe, "Label-Free Biosensor Based on an All-Polymer DFB Laser," *Advanced Optical Materials*, vol. 2, no. 2, pp. 137-141, Jan, 2014.
- [15] K. Kurihara, H. Ohkawa, Y. Iwasaki, O. Niwa, T. Tobita, and K. Suzuki, "Fiber-optic conical microsensors for surface plasmon resonance using chemically etched single-mode fiber," *Analytica Chimica Acta*, vol. 523, no. 2, pp. 165-170, Oct, 2004.
- [16] X. Fan, I. M. White, S. I. Shopova, H. Zhu, J. D. Suter, and Y. Sun, "Sensitive optical biosensors for unlabeled targets: A review," *Analytica Chimica Acta*, vol. 620, no. 1-2, pp. 8-26, Jul, 2008.
- [17] Y. Zhao, X. G. Li, L. Cai, and Y. Yang, "Refractive index sensing based on photonic crystal fiber interferometer structure with up-tapered joints," *Sensors and Actuators B-Chemical*, vol. 221, pp. 406-410, Dec, 2015.
- [18] Z. B. Tian, S. S. H. Yam, and H. P. Loock, "Single-mode fiber refractive index sensor based on core-offset attenuators," *IEEE Photonics Technology Letters*, vol. 20, no. 13-16, pp. 1387-1389, Jul, 2008.
- [19] H. Q. Cheng, Z. G. Jing, P. Wei, and C. Q. Xing, "Temperature compensation fiber-optic Refractive Index Sensor based on single-mode fiber core-offset Attenuator," *22nd International Conference on Optical Fiber Sensors, Pts 1-3*, vol. 8421, Nov, 2012.
- [20] Z. B. Tian, S. S. H. Yam, J. Barnes, W. Bock, P. Greig, J. M. Fraser, H. P. Loock, and R. D. Oleschuk, "Refractive index sensing with Mach-Zehnder interferometer based on concatenating two single-mode fiber tapers," *IEEE Photonics Technology Letters*, vol. 20, no. 5-8, pp. 626-628, Mar, 2008.
- [21] Z. Li, C. Liao, D. Chen, J. Song, W. Jin, G.-D. Peng, F. Zhu, Y. Wang, J. He, and Y. Wang, "Label-free detection of bovine serum albumin based on an in-fiber Mach-Zehnder interferometric biosensor," *Optics Express*, vol. 25, no. 15, pp. 17105-17113, Jul, 2017.
- [22] D. Wu, Y. Huang, J.-Y. Fu, and G.-Y. Wang, "Fiber Fabry-Perot tip sensor based on multimode photonic crystal fiber," *Optics Communications*, vol. 338, pp. 288-291, Mar, 2015.
- [23] M. Quan, J. Tian, and Y. Yao, "Ultra-high sensitivity Fabry-Perot interferometer gas refractive index fiber sensor based on photonic crystal fiber and Vernier effect," *Optics Letters*, vol. 40, no. 21, pp. 4891-4894, Nov, 2015.
- [24] P. Hlubina, M. Kadulova, D. Ciprian, and J. Sobota, "Reflection-based fibre-optic refractive index sensor using surface plasmon resonance," *Journal of the European Optical Society: Rapid Publications*, vol. 9, pp. 14033-5, Aug, 2014.
- [25] Z. Liu, Y. Wei, Y. Zhang, Y. Zhang, E. Zhao, J. Yang, and L. Yuan, "Twin-core fiber SPR sensor," *Optics Letters*, vol. 40, no. 12, pp. 2826-9, Jun, 2015.
- [26] X. Fang, C. R. Liao, and D. N. Wang, "Femtosecond laser fabricated fiber Bragg grating in microfiber for refractive index sensing," *Optics Letters*, vol. 35, no. 7, pp. 1007-1009, Apr, 2010.
- [27] M. Han, F. W. Guo, and Y. F. Lu, "Optical fiber refractometer based on cladding-mode Bragg grating," *Optics Letters*, vol. 35, no. 3, pp. 399-401, Feb, 2010.
- [28] S. C. Warren-Smith, R. Kostecki, L. V. Nguyen, and T. M. Monro, "Fabrication, splicing, Bragg grating writing, and polyelectrolyte functionalization of exposed-core microstructured optical fibers," *Optics Express*, vol. 22, no. 24, pp. 29493-29504, Dec, 2014.
- [29] D. J. J. Hu, J. L. Lim, M. Jiang, Y. X. Wang, F. Luan, P. P. Shum, H. F. Wei, and W. J. Tong, "Long period grating cascaded to photonic crystal fiber modal interferometer for simultaneous measurement of temperature and refractive index," *Optics Letters*, vol. 37, no. 12, pp. 2283-2285, Jun, 2012.
- [30] Q. Wu, H. P. Chan, J. Yuan, Y. Ma, M. Yang, Y. Semenova, B. Yan, P. Wang, C. Yu, and G. Farrell, "Enhanced refractive index sensor using a combination of a long period fiber grating and a small core singlemode fiber structure," *Measurement Science and Technology*, vol. 24, no. 9, pp. 094002, Jul, 2013.
- [31] Y. Huang, B. Chen, G. Chen, H. Xiao, and S. U. Khan, "Simultaneous detection of liquid level and refractive index with a long-period fiber grating based sensor device," *Measurement Science and Technology*, vol. 24, no. 9, pp. 095303, Jul, 2013.
- [32] C. Y. Han, H. Ding, X. L. Li, and S. F. Dong, "Temperature insensitive refractive index sensor based on single-mode micro-fiber Sagnac loop interferometer," *Applied Physics Letters*, vol. 104, no. 18, May, 2014.
- [33] A. Francois, and M. Himmelhaus, "Optical biosensor based on whispering gallery mode excitations in clusters of microparticles," *Applied Physics Letters*, vol. 92, no. 14, pp. 141107, Apr, 2008.
- [34] K. Kosma, G. Zito, K. Schuster, and S. Pissadakis, "Whispering gallery mode microsphere resonator integrated inside a microstructured optical fiber," *Optics Letters*, vol. 38, no. 8, pp. 1301-1303, Apr, 2013.
- [35] P. Chen, X. Shu, H. Cao, and K. Sugden, "High-sensitivity and large-dynamic-range refractive index sensors employing weak composite Fabry-Perot cavities," *Optics Letters*, vol. 42, no. 16, pp. 3145-3148, Aug, 2017.
- [36] X. Li, L. V. Nguyen, Y. Zhao, H. Ebendorff-Heidepriem, S. Warren-Smith, High-sensitivity Sagnac-interferometer biosensor based on exposed core microstructured optical fiber. *Sensors and Actuators B: Chemical*. vol. 269, pp. 103-109, Sep. 2018.
- [37] Y. Cardona-Maya, I. Del Villar, A.B.Socorro, J.M.Corres, I.R. Matias, and J.F. Botero-Cadavid, "Wavelength and phase detection based SMS fiber sensors optimized with etching and nanodeposition," *Journal of Lightwave Technology*, vol. 35, no. 17, pp. 3743-3749, Sep, 2017
- [38] J. Silverstone, S. McFarlane, C. Manchee, and A. Meldrum, "Ultimate resolution for refractometric sensing with whispering gallery mode microcavities," *Optics Express*, vol. 20, no. 8, pp. 8284-8295, Apr. 2012.
- [39] R. Kostecki, H. Ebendorff-Heidepriem, C. Davis, G. McAdam, S. C. Warren-Smith, and T. M. Monro, "Silica exposed-core microstructured optical fibers," *Optical Materials Express*, vol. 2, no. 11, pp. 1538-1547, Nov, 2012.
- [40] W. M. Haynes, *CRC handbook of chemistry and physics*: CRC press, 2014.
- [41] X.Fan, I.M. White, S.I. Shopova, H.Zhu, J.D. Suter, and Y. Sun, "Sensitive optical biosensors for unlabeled targets: A review," *Analytica Chimica Acta*, vol. 620, no. 1-2, pp.8-26, July, 2008.
- [42] S. Chandran, and R. Singh, "Comparison of various international guidelines for analytical method validation," *Die Pharmazie-An International Journal of Pharmaceutical Sciences*, vol. 62, no. 1, pp. 4-14, Jan, 2007.

Xue-gang Li received his B.A. degrees in the College of Information Science and Engineering from the Northeastern University, China, in 2014. He is now a visiting PhD student of the University of Adelaide. His research interests are photonic crystal fiber sensors, optical modal interference sensors, in-fiber interferometer and its sensing applications. He has authored and co-authored more than ten scientific papers.

Stephen C. Warren-Smith completed his PhD in 2011 at the University of Adelaide, Australia, on the topic of microstructured optical fiber chemical sensing. He was then employed from 2011 to 2014 as an Australian Research Council (ARC) Super Science Fellow at the Institute for Photonics and Advanced Sensing and the School of Chemistry and Physics at the University of Adelaide, working on optical fiber biosensing for women's health applications. In 2015 and 2016 he worked as a European Union Marie Curie International Incoming Fellow at the Institute of Photonic Technology, Jena, Germany, on a project investigating the micro/nano-structuring of optical fibers for sensing. Since October 2016 he is with the University of Adelaide as a Ramsay Fellow.

Heike Ebendorff-Heidepriem obtained her PhD in chemistry from the University of Jena, Germany in 1994 and subsequently held two prestigious fellowships. From 2001-2004 she was with the Optoelectronics Research Centre at the University of

> REPLACE THIS LINE WITH YOUR PAPER IDENTIFICATION NUMBER (DOUBLE-CLICK HERE TO EDIT) <

10

Southampton, UK. Heike came to the University of Adelaide in 2005. She was awarded the Woldemar A. Weyl International Glass Science Award in 2001, the International Zwick Science Award in 2009 and the University of Adelaide Women's Research Excellence Mid-Career Award in 2014. Heike has published over 230 refereed journal papers and conference proceedings, including 5 review papers and 9 postdeadline papers, and raised approximately \$12M for research. Heike's research focuses on the development of novel optical glasses, fibers, surface functionalization and sensing approaches.

Ya-Nan Zhang received the M.A. and Ph.D. degrees from the College of Information Science and Engineering, Northeastern University, Shenyang, China, in 2012 and 2015, respectively. She is currently an Associate Professor with Northeastern University. She has authored or co-authored more than 30 scientific papers and conference presentations. Her current research interests include optical fiber sensors, photonic crystal sensors, slow light technology, and its sensing applications.

Linh V. Nguyen was born in Hanoi, Vietnam. After graduating with a BSc. degree in Applied Physics from Hanoi University of Science in 2002 he moved to South Korea and earned a PhD in Information and Communications from Gwangju Institute of Science and Technology (GIST), South Korea, in 2009. His graduate works focused on the development of fiber-optics devices for applications in fiber sensor, fiber laser and all-optical signal processing. In early 2010 he moved to Edith Cowan University (ECU) in Western Australia to work on the development of fiber-optics sensors for applications in Desalination and seawater-related industries. His experiences range from fabrication (MCVD, DT) and characterization of specialty optical fiber to development of fiber devices (grating, sensor, laser, micro-machined fiber, etc). In 2011 he joined the Institute for Photonics & Advanced Sensing (IPAS), School of Physical Sciences at the University of Adelaide in 2011, first as an Australian Research Council (ARC) Super Science Fellow leading a project toward development of rapid protein sensing and blood typing platform at crime scenes, and subsequently as a Research Associate on a project developing of tools for in-field surveillance of pathogens.